

# Modeling of fluctuating interaction energy between a gliding interstitial cluster and solute atoms in random binary alloys

著者	Satoh Y., Abe H., Matsunaga T.
journal or publication title	Philosophical Magazine
volume	93
number	14
page range	1652-1676
year	2012-12-14
URL	<a href="http://hdl.handle.net/10097/63880">http://hdl.handle.net/10097/63880</a>

doi: 10.1080/14786435.2012.752884

*This is an Accepted Manuscript of an article published by Taylor & Francis Group in Philosophical Magazine on 14/12/2012, available online:*  
<http://www.tandfonline.com/10.1080/14786435.2012.752884>.

Philosophical Magazine, 93 (2013) pp. 1652–1676.

## **Modeling of fluctuating interaction energy between a gliding interstitial cluster and solute atoms in random binary alloys**

Y. Satoh, H. Abe, T. Matsunaga

*Institute for Materials Research, Tohoku University, 2-1-1 Katahira, Aoba-ku, Sendai 980-8577, Japan*

### **Abstract**

Fluctuation in microscopic distribution of solute atoms will act as a barrier for glide motion (i.e. 1D migration) of interstitial clusters in random alloys. We proposed an analytical model in which the total interaction energy between an interstitial cluster and solute atoms is a superposition of the interaction potential between the cluster and individual solute atom. Then we examined the nature of fluctuation in the total interaction energy of a gliding cluster. The average amplitude of the fluctuation was directly proportional to the square root of both the solute concentration  $c_s$  and the cluster radius  $r_c$ . The distance separating local peaks in the fluctuation was virtually independent of  $c_s$  and  $r_c$ , but showed dependence only on the range of the interaction potential. We proposed a model for another fluctuation in the interaction energy because of solute–solute interaction that is effective at high  $c_s$ . The models interpreted the results of the molecular statics simulations of the fluctuating interaction energy for interstitial clusters (7i, 61i, and 217i) in dilute and concentrated Fe-Cu alloys with random solute distribution. We proposed that the fluctuation in the interaction energy is responsible for the short-range 1D migration that is observed in various alloys in electron irradiation experiments. The distance between local peaks would give the characteristic length of 1D migration in concentrated alloys.

## 1. Introduction

Clusters of self-interstitial atoms appear in the form of platelet in various metals irradiated with high-energy particles. Typical nucleation of interstitial clusters occurs through migration and agglomeration of single interstitial atoms during high-energy electron irradiation. Clusters of up to a few tens of interstitial atoms are regarded as forming directly from large collision cascades under high-energy neutron irradiation [1-3]. Interstitial clusters tend to grow large with absorption of interstitial atoms under irradiation at high temperatures, although fine-scale clusters accumulate at high densities at low temperatures. A recent study of radiation damage for materials development of future nuclear power applications revealed that the nature and behavior of small interstitial clusters have practical importance in two respects. Small interstitial clusters as well as small precipitates induced by the irradiation act as obstacles against dislocation motion and are responsible for irradiation-hardening. In addition, small interstitial clusters cause glide motion along the direction of the Burgers vector with low activation energy, called one-dimensional (1D) migration [4-6], which is considered to affect defect structural evolution. A small interstitial cluster is regarded as a ‘bundle of crowdions’, and the cluster changes to an interstitial-type dislocation loop with increasing cluster size. Analysis of the strain field of the cluster and of interaction between the cluster and vacancies suggest that the border of both clusters lays around 200 interstitial atoms in iron and nickel [7]. Both types of interstitial clusters are considered to cause fast 1D migration, and are called interstitial clusters in this paper.

In situ observation using high-voltage electron microscopy (HVEM) is an efficient experimental method for investigating basic processes of 1D migration of interstitial clusters because 1D migration is induced by irradiation with high-energy electrons [8-15]. The typical 1D migration observed in iron is stepwise positional changes occurring at irregular intervals, which often involve fast back-and-forth motion. It differs from typical 1D migration observed in atomistic simulations for pure iron based on molecular dynamics (MD) method, i.e., fast 1D random walks with low activation energy [5,6,16]. Considerable mechanisms for the difference have been discussed in terms of interaction of interstitial clusters with other interstitial clusters [8-10], vacancies [17], vacancy clusters [18], impurity atoms [11,12,19], and impurity–vacancy complex [20]; a low-symmetry (‘non-parallel’) configuration in interstitial clusters [21], and impact with fast electrons [11,22].

1D migration processes in alloys containing both substitutional and interstitial solute/impurity atoms at high concentration are of fundamental and technical importance. 1D migration of interstitial clusters has not been reported in alloys with conventional 200 kV TEM. In situ observation with HVEM has revealed frequent 1D migration at irregular intervals under electron irradiation in commercial alloys and high-purity model alloys [9,10,13-15]. The frequency of 1D migration is almost in direct proportion to the electron beam intensity [14]. The distance of 1D migration in these alloys is shorter than that in iron, and hardly exceeds 10 nm [9,10,13-15]. Among the SUS316L and its high-purity model alloys, no clear difference is observed in the frequency or distance of 1D migration under irradiation at room temperature, suggesting that the fundamental mechanism of the 1D migration is related to major alloying elements rather than minor solute/impurity atoms [14].

In random alloys, because of fluctuation in microscopic distribution of solute atoms, total interaction energy between an interstitial cluster and solute atoms fluctuates with the glide distance of the cluster, which will act as barriers for 1D migration. Examination of the characteristics of the fluctuation in the interaction energy in random binary alloys will contribute to the understanding and modeling of 1D migration processes in alloys. Cottrell et al. [23] first proposed a model for this subject with application of a general concept of solution hardening. The model took account only of short-range interactions, i.e., solute atoms in the central core of the loop dislocation. The present study adopted another approach for the subject. We assumed the total interaction energy to be a superposition of long-range potentials for interaction between the interstitial cluster and individual solute atom. We then analyzed the amplitude and wavelength of the fluctuation in the total interaction energy. Next we examined an applicability of the model using molecular statics (MS) simulations for Fe-Cu alloys under typical conditions for solute concentration and cluster radius. We examined also a contribution of solute-solute interaction to the total interaction energy. This study was undertaken to contribute to the elucidation and modeling of 1D migration processes of interstitial clusters in practical alloys. The findings of this study were expected to engender a more precise understanding and modeling of microstructural evolution upon energetic particle irradiation.

## **2. Model for interstitial clusters in binary alloys**

## 2.1. Interaction between an interstitial cluster and solute atoms

We proposed an analytical model for the total interaction energy between an interstitial cluster and solute atoms in binary alloys, as shown schematically in Figure 1. Strong interaction is expected for the solute atoms in a central core of the loop dislocation. Letting the cross section of the annular region be  $\sigma$  (expressed by the number of atoms contained in the region), and letting the thickness be  $b$  (i.e. the atomic distance), then the volume of the region is  $\sigma b$  atoms. The cross section  $\sigma$  will be in proportion to the length of the loop dislocation. The number of solute atoms  $n(x)$  in the region fluctuates with position  $x$  of the cluster that glides along the direction of the Burgers vector. We consider also the weak interaction with solute atoms near the annular region by assuming an interaction potential  $u_{\text{peak}} f(v)$ , where  $u_{\text{peak}}$  is the peak interaction energy and  $f(v)$  is a non-dimensional function of the distance  $v$  between the solute atom and the annular region in the  $x$  direction. The function is  $f(0) = 1$ , which decreases monotonically with increasing distance  $v$ , and which is effectively  $f(v) = 0$  for  $|v| > w$ ; the interaction range  $w$  will be approximately  $10b$ . The positive and negative values for  $u_{\text{peak}}$  respectively represent repulsive and attractive interactions.

For simplicity, we assume an identical interaction potential  $u_{\text{peak}} f(v)$  for all solute atoms the projection of which along  $x$  direction are on the annular region, and ignore the other solute atoms. The total interaction energy in a solid solution is assumed to be given by a simple superposition of interaction potentials for individual solute atom, thereby by a convolution integral of the two functions as

$$u(x) = u_{\text{peak}} \int_{-w}^w f(v) n(x-v) dv . \quad (1)$$

Characteristics of the fluctuation in the total interaction energy  $u(x)$  are examined in the following sections.

## 2.2. Outlines of the total interaction energy

The three functions presented above are considered at discrete points with an interval  $b$  in the respective finite periods of  $n_j = n(jb)$  and  $u_j = u(jb)$  for  $j = 0, 1, \dots, L-1$ ;  $f_j = f(jb)$  for  $j = -L/2, \dots, -1, 0, 1, \dots, L/2-1$ . Parameter  $L$ , an even number, is sufficiently large that  $Lb \gg w$ . Using linear convolution, Eq. (1) is written

as

$$u_j = u_{\text{peak}} \sum_{q=-\frac{L}{2}}^{\frac{L-1}{2}} f_q n_{j-q}. \quad (1')$$

Figure 2(a) portrays outlines of the three functions in a random alloy for solute concentration  $c_s$ .

- (1) The interaction potential is approximated as a Gaussian function

$$f(v) = \exp(-v^2/\alpha^2), \quad (2)$$

where  $\alpha (> 0)$  is a constant representing the interaction range. The interaction energy decreases to  $u_{\text{peak}} e^{-1}$  at  $v = \pm\alpha$ . The figure shows cases for  $\alpha = 3b$  and  $\alpha = 7b$ .

- (2) The number of solute atoms  $n_j$  in the annular region fluctuates with the migration distance of the interstitial cluster. Statistically,  $n_j$  follows the binomial

distribution  $P_b(n, \sigma, c_s) = C_n c_s^n (1 - c_s)^{\sigma - n}$ , which has average and variance as

shown below:

$$E[n] = \sigma c_s, \quad V[n] = \sigma c_s (1 - c_s). \quad (3)$$

- (3) The total interaction energy  $u_j$ , a superposition of interaction potentials, shows periodic fluctuation with local peaks, i.e., smooth hills and valleys. The relation between  $n_j$  and  $u_j$  is understood from the perspective that the convolution operation in Eq. (1') is a 'moving average' of  $n_j$  using  $f_j$  as weights. Because weight  $f_j$  is a smoothing function, the averaging filters out fine scale fluctuations in  $n_j$ , and the trend remains in  $u_j$ . Larger  $\alpha$  averages over a longer range and results in smoother profiles.

### 2.3. Fourier spectrum of the total interaction energy

The three functions are described using Fourier analysis. Let  $F_k$ ,  $N_k$ , and  $U_k$  respectively denote the coefficients of discrete Fourier transforms of the functions  $f_j$ ,

$n_j$ , and  $u_j$ . In the present convention, the discrete Fourier transform is, for example,

$$U_k = \frac{1}{L} \sum_{j=0}^{L-1} u_j e^{-i\frac{2\pi}{L}kj} \quad k = 0, 1, \dots, L-1. \quad (4)$$

It denotes the complex amplitude of the wave having wavelength  $\lambda = bL/k$ . Also,  $i$  is an imaginary unit. Figure 2(b) presents outlines of the amplitude spectra in half of the frequency space because Fourier coefficients of real-valued functions are symmetrical at  $k = 0$ .

- (1) The Fourier transform of the function  $f_j$  for the interaction potential is another Gaussian function of real value, as

$$F_k = \frac{\pi^{\frac{1}{2}} \alpha}{bL} \exp\left(-\frac{\pi^2 \alpha^2}{b^2 L^2} k^2\right) \quad k = 0, 1, \dots, L-1. \quad (5)$$

The spectrum involves a monotonic decrease at higher spatial frequencies.

- (2) The number of solute atoms  $n_j$  shows random fluctuation. Therefore, its Fourier transform has uniform intensity for all spatial frequencies except for  $k = 0$ . It is analogous to that of white noise as a function of time. The uniform power spectrum is expressed using the solute concentration  $c_s$  and the interaction cross-section  $\sigma$  (see Appendix A for the derivation), as

$$|N_k|^2 = \frac{V[n]}{L-1} = \frac{\sigma c_s (1-c_s)}{L-1} \quad k = 1, 2, \dots, L-1. \quad (6)$$

- (3) A convolution operation in the spatial domain is expressed as a product in the frequency domain. Eq. (1') is written as

$$U_k = u_{\text{peak}} L F_k N_k. \quad (7)$$

From Eqs. (5), (6), and (7), we obtain the intensity of the Fourier transform as

$$|U_k|^2 = \frac{\sigma c_s (1-c_s)}{L-1} \frac{\pi u_{\text{peak}}^2 \alpha^2}{b^2} \exp\left(-\frac{2\pi^2 \alpha^2}{b^2 L^2} k^2\right) \quad k = 1, 2, \dots, L-1. \quad (8)$$

The exponential term in Eq. (8) represents the frequency dependence of the

spectrum that is related to the wavelength of the smooth fluctuation in  $u_j$ . Therein,  $|U_k|$  and  $|F_k|$  have an identical frequency dependence because of the uniform spectrum in  $|N_k|$ . In this sense, the characteristics of the fluctuation in  $u_j$  are analogous to those of white noise processed with a low-pass filter. In contrast, the pre-exponential factor in Eq. (8), which represents the overall intensity level of the spectrum, is directly proportional to the square of the average amplitude of the fluctuation in  $u_j$ , as

$$V[u] = \sum_{k=1}^{L-1} |U_k|^2 \approx \frac{\sigma c_s (1 - c_s)}{L - 1} \frac{\pi u_{\text{peak}}^2 \alpha^2}{b^2} \left( \frac{bL}{\sqrt{2\pi\alpha}} - 1 \right) \approx \sqrt{\frac{\pi}{2}} \frac{\sigma c_s (1 - c_s) u_{\text{peak}}^2 \alpha}{b}. \quad (9)$$

#### 2.4. Variation of the total interaction energy

Figure 3 presents typical variation of  $n_j$  and  $u_j$  with the solute concentration  $c_s$ . In dilute alloys for  $\sigma c_s \ll 1$ , the annular region contains no solute atom or occasionally a single solute atom with probabilities  $P(0) = 1 - \sigma c_s$  and  $P(1) = \sigma c_s$ , respectively [11]. The total interaction energy  $u_j$  has isolated peaks corresponding to solute atoms in the annular region. The height of peaks is  $u_{\text{peak}}$ , and the mutual distance  $xb$  obeys the geometrical distribution  $P_g(x, \sigma c_s) = \sigma c_s (1 - \sigma c_s)^{x-1}$ , as described in a previous report [11].

As the solute concentration increases to  $c_s \approx 1/(2\alpha\sigma)$ , respective peaks mutually overlap. Further overlapping at higher  $c_s$  does not flatten the energy profile but increases the fluctuation amplitude. Eq. (9) shows that  $V[u]^{1/2}$  is in proportion to  $c_s^{1/2} (1 - c_s)^{1/2}$ ; note  $c_s^{1/2} (1 - c_s)^{1/2} \approx c_s^{1/2}$  for  $c_s$  much lower than 50 atomic percent. The average amplitude of the fluctuation  $V[u]^{1/2}$  is also proportional to the peak interaction energy  $u_{\text{peak}}$ , and to the square root of the interaction cross section  $\sigma^{1/2}$ . We note that the relation reflects a fluctuation in the total number of solute atoms interacting with the loop dislocation. On the other hand, Eq. (8) shows that the wavelength of the fluctuation is independent of  $c_s$  or  $\sigma$ , but only on parameter  $\alpha$  for the interaction range. Therefore, as a statistical average,  $u_j$  varies only in the scale of the vertical axis in proportion to  $c_s^{1/2} (1 - c_s)^{1/2}$ , which is also readily apparent in Figure 3(b).



Figures 4(a) and 4(b) show distributions of the energy difference  $E_p$  and the distance  $d_p$  between the neighboring local peaks (i.e., hills and valleys) in the total interaction energy  $u_j$ . Distance  $d_p$  has a unique distribution when it is normalized by the interaction range  $\alpha$ . Again it does not depend on  $c_s$  or  $\sigma$ . The energy difference  $E_p$  has another unique distribution when it is normalized by  $V[u]^{1/2}$ .

### 3. Atomistic simulations for the model

#### 3.1. Description of the calculation cell

We conducted atomistic simulations of the interaction energy based on the MS method to examine the applicability of the analytical model proposed in Sec. 2. We selected Fe-Cu system with an interatomic potential given by Ackland et al. [24] that has been used for simulations of 1D migration [11,25,26]. The volume size factor of the solute copper atom in the iron lattice is about +8.8% in this potential function [24]. We induced solute copper atoms at random at concentrations up to 70 atomic percent to compare the results with the proposed model under various conditions. Although a random alloy is unrealistic at high solute concentrations because of low solubility of copper in iron, this study regards the system as an example of binary alloys. Hamaoka et al. conducted the HVEM experiments of 1D migration in Fe-Cu alloys from 0.005 to 0.9 at.%Cu [15].

The calculation cell contained about  $1.3 \times 10^6$  mobile atoms, as shown in Figure 5(a). A periodic boundary condition was applied for all faces of the calculation cell at zero pressure. An interstitial cluster of a hexagonal plate was introduced at the cell center. The maximum radius  $r_c$  of the interstitial cluster was 1b (7i), 4b (61i), or 8b (217i), as shown in Figure 5(b). Atoms on a hexagonal shell were grouped and labeled by the maximum radius  $r_h$  of the shell. For example, all atoms on the edge of the interstitial cluster 217i belong to a shell for  $r_h = 8b$ .

#### 3.2. Interaction between an interstitial cluster and a single solute copper atom

An interstitial cluster was fully relaxed in the iron lattice using the MS method. Then an iron atom in the cell was replaced by a copper atom. The interaction energy was estimated from the change in the total formation energy of the cell after relaxation. The typical error in estimating the formation energy was not larger than 0.005 eV. Each

symbol in Figure 6(a) designates the interaction energy between an interstitial cluster (217i) and a solute atom in individual atomic row that is shown with broken circles in Figure 5(b), which corresponds to  $u_{\text{peak}} f_i$  in the model presented in Sec. 2. Bold lines in Figure 6(a) are Gaussian functions fitted to the calculated results, with adoption of appropriate values for peak energy  $u_{\text{peak}}$  and parameter  $\alpha$  for the interaction range. The interaction is repulsive for the solute atom in the atomic rows inside the loop dislocation ( $r_h < 8b$ ) because of the compressional strain, and is attractive on the outside ( $r_h > 8b$ ). The interaction is slight on the edge of the cluster ( $r_h = 8b$ ). Results for 7i were described in earlier reports [11,26]. Figures 6(b) and 6(c) summarize the parameters  $u_{\text{peak}}$  and  $\alpha$  for the three cluster radii. They have similar variation to that shown against  $r_h - r_c$ , the radial distance from the dislocation core. The difference in  $u_{\text{peak}}$  was less than 0.022 eV for atomic rows between edge and corner positions (shown with broken circles and a box, respectively in Figure 5(b)) within a hexagonal shell from  $r_h = 6b$  to  $12b$  in 217i. These results suggest that the long-range interaction between the cluster and a solute atom is described better by defining the interaction potential for an individual shell.

### 3.3. Interaction energy in random Fe-Cu alloys

We calculated the total interaction energy corresponding to  $u_j$  in Sec. 2 according to the MS method shown schematically in Figure 5(c):

- (1) The initial formation energy of the calculation cell is denoted as  $E_j^a$ .
- (2) The solute atoms in the single atomic layer at the cell surface,  $0 \leq x < b$  (shaded region in Figure 5(c)), were replaced by those with a new random distribution. The formation energy of the cell after relaxation was  $E_j^b$ . The difference  $E_j^b - E_j^a$  resulted from the change in the number and the distribution of solute atoms in the surface layer. The interstitial cluster was far from the layer. Therefore, this treatment was assumed not to affect the interaction energy between the cluster and solute atoms.
- (3) The distribution of all the solute atoms in the cell was translated toward  $-x$  direction for a distance  $b$ . This operation was done by switching the parameters indicating atomic species without changing the atom coordinates. The formation energy of the cell after relaxation was  $E_{j+1}^a$ . The difference  $E_{j+1}^a - E_j^b$  was equivalent to the net change in the interaction energy of the cluster that migrates for

a distance  $b$  toward  $+x$  direction,  $u_{j+1} - u_j = E_{j+1}^a - E_j^b$ .

An iteration of the sequence produced a total interaction energy profile longer than the size of the calculation cell (i.e. 120 b) while introducing random solute distributions. Bold lines in Figure 7 show typical profiles of the interaction energy. The amplitude of the fluctuation in the interaction energy exceeded a few electron volts in concentrated alloys, even though the energy of the individual interaction potential was around 0.1 eV. The fluctuation will act as barriers for 1D migration of interstitial clusters larger than a few nano-meters.

### 3.4. Comparison between MS simulation and the analytical model

Thin lines in Figure 7 show the interaction energy in which interaction potentials  $u_{rh, \text{peak}} f_{rh, j}$  were superposed according to the solute distribution  $n_{rh, j}$  used in the MS calculation as

$$u_j = \sum_{rh} u_{rh, \text{peak}} \sum_{q=-\frac{L}{2}}^{\frac{L}{2}-1} f_{rh, j} n_{rh, j-q}. \quad (1'')$$

Suffix  $rh$  implies that the functions are defined for an individual hexagonal shell with radius  $r_h$ . The interaction potential  $u_{rh, \text{peak}} f_{rh, j}$  was produced with interpolation of

parameters  $u_{rh, \text{peak}}$  and  $\alpha_{rh}$  shown in Figures 6(b) and 6(c). The superposition

reproduces the MS results at low  $c_s$ , but only the position and shape of individual local peak at high  $c_s$ . Comparison of the two profiles at low magnification (Fig. 7(a)) reveals that the discrepancy at high  $c_s$  results from slow fluctuation involved in the results of MS calculation. We describe in Sec. 4A that slow fluctuation arose from interaction among solute atoms (shown by dotted lines in Figure 7). We show in the following that the amplitude and wavelength of the fluctuation in  $u_j$  are fundamentally consistent with the analytical model.

The symbols and lines presented in Figure 8(a) show a comparison of the average amplitude of the fluctuation  $\sqrt{V[u]}^{1/2}$  between the MS calculation and the superposed interaction potentials. The latter was given by a sum of the variances for an individual shell as

$$V[u] \approx \sqrt{\frac{\pi}{2}} \frac{c_s(1-c_s)}{b} \sum_{rh} \alpha_{rh} \sigma_{rh} u_{rh, \text{peak}}^2, \quad (9')$$

because the contribution of the individual shell to the total variance was mutually independent. The average amplitude of the fluctuation  $V[u]^{1/2}$  for multiple shells is directly proportional to  $c_s^{1/2}(1-c_s)^{1/2}$ . The two results show good correspondence at  $c_s$  lower than several atomic percent.

Shaded bars and bold lines in Figure 9(a) respectively show Fourier spectra  $|U_k|$  of the total interaction energy obtained using the MS calculation and the superposition. The two spectra show good correspondence at high frequencies. The discrepancy observed at very low frequencies is again caused by the contribution of the slow fluctuation of the solute–solute interaction, as shown by dotted lines in Figure 9(a). The spectra for the superposition have similar frequency dependence, which are probably reproduced by an appropriate blending of the spectra for Gaussian functions from  $\alpha = 3b$  to  $10b$  shown in Figure 9(b).

The energy difference  $E_p$  and distance  $d_p$  of the neighboring peaks were measured in the total interaction energy  $u_j$  obtained using the MS calculation. Figure 10(a) presents broad distributions of the energy difference  $E_p$ , whereas Figure 8(b) shows that the average  $E_p$  is almost proportional to  $r_c^{1/2}$  and  $c_s^{1/2}$ . Effects of the slow fluctuation caused by solute–solute interaction were less apparent on the average  $E_p$  than on  $V[u]^{1/2}$  shown in Figure 8(a). Figure 10(b) shows that  $d_p$  is 0.5–2 nm, and that its distribution apparently does not depend on  $c_s$  or  $r_c$ . These results are fundamentally consistent with the simple model, except for the difference in the distribution of  $d_p$ . The fraction at short  $d_p$  is larger for the MS results (Fig. 10(b)) than the simple model (Fig. 4(b)). The difference might be attributed to the interference of Gaussian functions among different  $u_{\text{peak}}$  and  $\alpha$  in the MS calculation. Finally, we note a correlation between the energy difference  $E_p$  and the distance  $d_p$ ; local peaks with longer  $d_p$  tend to have larger  $E_p$ , as shown in Figure 10(b). The correlation is understood from the Fourier spectra: the lower amplitude at higher frequency allows only a smooth fluctuation in the spatial domain.

## 4. Discussion

### 4.1. Solute–solute interaction

Solute–solute interaction was ignored in the model described above. The interaction energy between two solute atoms was estimated from changes in the total formation energy of the calculation cell containing two solute atoms at various distances. The energy was -0.075 eV [24], -0.035 eV [24], and +0.020 eV, respectively, for pairs of the first-, second-, and third-nearest distances in the iron lattice; it was negligible for more distant pairs. The negative values denote attractive interactions. In this section, fluctuation in the solute–solute interaction energy of migrating interstitial clusters was examined to elucidate the characteristics of fluctuation in the total interaction energy, especially at higher  $c_s$ .

1D migration of an interstitial cluster is regarded as a glide of the loop dislocation on the cylindrical glide plane. Simultaneously, the two parts of the crystal, i.e., inside and outside the glide cylinder, shift from each other by distance  $b$  along the Burgers vector. Figure 11(a) portrays configurational changes of close solute pairs as the interstitial cluster migrates leftward. It is noteworthy that the figure shows an interstitial cluster fixed and solute atoms relative to the cluster. The changes in the mutual distance of solute pairs will change the interaction energy. We estimated the fluctuation in the total energy of solute–solute interaction based on the following assumptions: 1) we considered only the solute pairs for which the ‘atomic bond’ lies across the glide plane as shown in the top row in Figure 11(a). 2) We ignored gradual variation in the bond distance as the dislocation core passed by the solute pair. Instead we identified the first-, second-, and third-nearest pairs in the two states without the distortion that is apparent long before and after the passage of the dislocation core. We assumed that the two states were exchanged stepwise at the closest approach of the dislocation core. The solute pairs shown in the top row in Figure 11(a) are to change from (i) to (iii) stepwise at the dislocation core (ii). Then the number of close solute pairs in the calculation cell fluctuates with every 1D migration for distance  $b$ . The fluctuation is a random walk process, as described quantitatively in Appendix B.

From the fluctuation in the number of close solute pairs of the first-, second-, and third-nearest distances and the respective interaction energies, we estimated the fluctuation in the total energy of solute–solute interaction and shown by dotted lines in

Figure 7. The number of close solute pairs is in direct proportion to  $c_s^2$ . Therefore, the fluctuation is negligible at low  $c_s$ . The sum of solute–defect interaction and solute–solute interaction is shown by broken lines, and better reproduces the MS results (bold lines) at high  $c_s$ . Consequently, the characteristics of the fluctuation in the Fe-Cu system are described using a filtered white noise for solute–defect interaction and random walk for solute–solute interaction. The total energy of solute–solute interaction fluctuates more slowly than that of solute–defect interactions. This slow fluctuation is also apparent in the Fourier spectra portrayed in Figure 9(a). The solute–defect interaction (bold lines) had larger amplitude than the solute–solute interaction (dotted lines) at high spatial frequencies. The range of 1D migration is limited by the fast fluctuation in the solute–defect interaction. The wavelength of the fluctuation will be the characteristic length of 1D migration in concentrated alloys.

#### 4.2. Solute–defect interaction

Interaction between a cluster and a single solute atom is the important element in the proposed model. In the classical theory of elasticity, the interaction energy between an inclusion at the cylindrical coordinate  $(r, z)$  and a circular dislocation loop of radius  $R$  at the origin is given as [27]

$$E = \frac{\delta V}{3\pi} \mu \frac{1+\nu}{1-\nu} \frac{b}{\sqrt{(R+r)^2 + z^2}} \left[ \frac{R^2 - r^2 - z^2}{(R-r)^2 + z^2} E \left( \sqrt{\frac{4rR}{(R+r)^2 + z^2}} \right) + K \left( \sqrt{\frac{4rR}{(R+r)^2 + z^2}} \right) \right], \quad (10)$$

where functions  $K(k)$  and  $E(k)$  are the complete elliptic integrals of the first and second kind. In addition,  $\mu$  and  $\nu$  respectively represent the shear modulus and Poisson's ratio. Only the size misfit  $\delta V$  is the variable parameter. The peak interaction energy depends on the misfit, but the interaction range does not. Thin lines in Figure 6(a) are interaction potentials for a solute atom with volume size factor of +15% in the iron lattice, which was chosen to correspond to the MS results in the atomic rows apart from the dislocation core,  $r_h = 0b$  and  $r_h = 12b$ . Near the dislocation core, however, Eq. (10) gives interaction potentials with larger peak energy and smaller width.

The singularities in the interaction energy at the dislocation core can be removed by introducing a constant  $A$  [28] into an expression for stress components of a circular dislocation loop [29]. Figure 12 (a) shows a variation of the interaction energy profiles

with the constant  $A$  for the atomic rows near the dislocation core. Profiles for  $A = 0$  are identical to those of Eq. (10) [27] that were shown by thin lines in Figure 6(a). The divergent behavior in the profile is suppressed with increasing  $A$ . It is reported that  $A \approx 0.1R$  produces suitable interaction energy profile for very small interstitial clusters (10i) [28]. For the present cluster (217i), profiles from  $A = 0.05R$  to  $A = 0.2R$  have the peak energy comparable to that of the MS results, but still have smaller peak width. We note that the elastic theory is better only for long-range interaction (i.e.,  $v \geq 7b$ ) inside the cluster  $r_h = 7b$ ; the Gaussian functions decay too fast for the long-range. The same observation applies to  $r_h = 6b$  and  $r_h = 3b$  in Figure 6 (a). Because the short-range interaction with larger energies has a large contribution to the total interaction energy, the Gaussian function will be a better approximation for the present case.

Symbols in Figure 12 (b) show interatomic distance along the Burgers vector in the atomic rows examined in Figures 6(a). Thin lines are those derived from the analytical solutions of the multistring Frenkel-Kontorova model for an edge dislocation and an interstitial cluster [30,31]: the atomic displacement of  $n$ -th atom in a string is given by  $u_n = (b/2) - (b/\pi) \arctan((n - n_0)/N)$ , where  $n_0$  is the index of the center atom of the crowdion. By adopting appropriate values for the parameter  $N$ , i.e., an effective dimensionless width of a crowdion, the solutions represent well the interatomic distance  $u_{n+1} - u_n + b$  of the atomic rows inside the cluster. A comparison between Figures 6(a) and 12(b) suggests a rough relation between the displacement field and the interaction energy. Results for 7i are available in earlier report [11]. However, precise interaction energy profiles would not be obtained from the displacement field. For example, the large displacement field observed in  $r_h = 8b$  does not result in significant interaction energy. This might be explained partly by displacement of the copper atom along the direction perpendicular to the Burgers vector; the oversized solute atom on the periphery of the interstitial cluster was found to displace outward for the distance around  $0.01b$ .

Density functional calculations suggest an importance of chemical interactions in addition to solute size factor for the interaction between a single interstitial atom in iron and a solute atom, depending on the solute elements [32]. For the interaction with an interstitial cluster, however, few reports describe atomistic simulations using

semi-empirical interatomic potentials. In a Ni-Au system, gold is an oversized solute atom in nickel with an extremely large volume size factor: 63.6%. The activation energy for an interstitial cluster (7i and 19i) to overcome a gold atom inside the cluster is 0.8–1.0 eV [33], which will correspond to  $u_{\text{peak}}$  in the system. Interaction in a Fe-Cr system is reported using an advanced semi-empirical potential that is parameterized by application of the density functional theory [34]. The sign of the interaction is opposite that of Fe-Cu system. The solute chromium atom inside a cluster (7i, 37i, or 91i) has attractive interaction, and the peak energy  $u_{\text{peak}}$  is from -0.1 to -0.2 eV for the solute atom on the edge of the cluster. We estimated that the interaction potential corresponds to  $\alpha = 4b$ .

### 4.3. Fluctuation in interaction energy in alloys

Cottrell et al. [23] analyzed the fluctuation in the total interaction energy of interstitial clusters in alloys with application of the theory of solid solution hardening [35]. In solution hardening, a flexible dislocation line of infinite length gains potential energy by adjusting its shape along valleys in a field of randomly arranged energy hills and valleys, where the dislocation must bow out at least the distance  $w$ , the range of interaction between dislocation and a solute atom. A critical length of dislocation segment, called the Labusch length, exists as

$$\xi_L = \left( \frac{Tw}{2\hat{U}c_s^{1/2}} \right)^{2/3}, \quad (11)$$

where  $T$  is the line tension and  $\hat{U}$  corresponds to  $|u_{\text{peak}}|$  in our notation. The fluctuation of potential energy on the scale  $\xi_L$  has amplitude of

$$E_L = \left( \frac{T}{2} \right)^{1/3} w^{4/3} \hat{U}^{2/3} c_s^{1/3}. \quad (12)$$

Dislocations can bow out only in scales larger than  $\xi_L$  because bowing out in smaller scales involves an increase in the line energy in excess of the gain in the potential energy. Such a dislocation is pinned by the fluctuation of the solute distribution, in the sense that the interaction energy must increase to pass over a hill-top into the next valley. The dislocation needs an external energy supply to move. In the solution



hardening the pinning energy is equivalent to the net energy gain. Cottrell et al. proposed the pinning energy for a dislocation loop of finite perimeter length  $nb$  under no driving stress acting on the loop [23],

$$E \approx E_L \left( \frac{nb}{\xi_L} \right)^{1/3}. \quad (13)$$

The pinning energy for 217i was estimated as 0.003, 0.09, and 0.26 eV for Fe-0.3%, 3%, and 30% Cu, respectively, with adoption of  $\hat{U} = 0.1 \text{ eV}$ ,  $nb = 50b$ ,  $w = 1b$ , and  $Tb = 1 \text{ eV}$  in Eqs. (11)–(13). The latter two parameters were after Cottrell et al. for iron-based alloys [23]. The pinning energies were much lower than the average  $E_p$  in the MS results presented in Figure 8(b). Parameter  $w = 1b$  represents a short-range interaction for solute atoms in the central core of the loop dislocation, ignoring the contribution of longer-range interaction. However, Figure 3 demonstrated a considerable difference in the interaction energy profiles between the short-range interaction  $u_{\text{peak}} n_j$  and the long-range interaction  $u_j$ . When we adopted  $w = 5b$ , the pinning energy increased to 0.20, 0.55, and 1.54 eV, respectively, which were comparable to the average  $E_p$ . We still note substantial differences between Cottrell's model and the MS results on Fe-Cu alloys: 1) We did not observe the loop dislocation to bow out in deflection as long as  $w = 5b$  during MD or MS simulations when we visualized the central core of the loop dislocation using the Wigner–Seitz cell method. 2) The typical pinning energy was directly proportional to  $c_s^{4/9} r_c^{1/3}$  in Cottrell's model but to  $c_s^{1/2} r_c^{1/2}$  for Fe-Cu alloys. The total interaction energy was interpreted better by the superposition of cluster–solute interaction and solute–solute interaction, neither of which considered the energy gain by bowing out of the loop dislocation.

#### 4.4. Brief comments

Fluctuation in the total interaction energy is expected to affect dynamic processes of 1D migration in alloys, depending on the temperature, species, concentrations of solute elements, and cluster size. Intermittent 1D migration is observed for interstitial clusters of a few nanometers in diameter under electron irradiation [9,10,13-15]. The 1D migration distance has a common distribution among the alloys examined. The fraction decreases concomitantly with increasing 1D migration distance, and the distance only slightly exceeds 10 nm. There would be a common mechanism for the distribution of

1D migration distance in these concentrated alloys. Our tentative model of experimental 1D migration is in the following. Interstitial clusters are in a stationary state in concentrated alloys, at a position where the formation energy of the clusters achieves a local minimum on their respective 1D migration tracks. The distribution of solute atoms is expected to change continuously from one random distribution to another (both are equivalent to each other) under electron irradiation because of displacement of atoms and the following recovery of produced Frenkel pairs. This ‘mixing’ effect of solute atoms changes the stable position of the cluster on its 1D migration track, and the clusters induce 1D migration into a new stable position. We presume that the experimental 1D migration distance reflects the wavelength of the fluctuation in the total interaction energy.

Atomistic simulations of diffusion coefficients of 1D migration have been reported for Fe-Cu and Fe-Cr alloys [25,36]. It is reported that the solute concentration dependence of 1D migration diffusivity ( $D_{1D}$ ) is not monotonous in Fe-Cr alloys; the diffusivity has a lower peak around 10 at.% Cr [36]. We have conducted dynamic simulations of 1D migration in Fe-Cu alloys in which we examined the behavior of interstitial clusters in terms of the fluctuation in the interaction energy. We also examined the mechanism of initiation of 1D migration under electron irradiation to elucidate the experimental 1D migration behavior in alloys. Those results will be presented elsewhere.

## **5. Conclusion**

For understanding and modeling of 1D migration of interstitial clusters in dilute and concentrated alloys, we studied characteristics of the fluctuation in the formation energy of interstitial clusters gliding along the Burgers vector. We proposed and examined two mechanisms of the fluctuation, which were solute–defect and solute–solute interactions, each of which reflects fluctuation in the microscopic distribution of solute atoms in terms of the cluster.

For the solute–defect interaction, the total interaction energy was assumed to be a superposition of a Gaussian function representing long-range interaction between the cluster and individual solute atom. An application of the model to random binary alloys revealed that the characteristics of the fluctuation resembled those of white noise processed with a low-pass filter. The average energy difference of the neighboring local

peaks in the fluctuation was directly proportional to the square root of both the solute concentration  $c_s$  and the cluster radius  $r_c$ . The distribution of the distance separating local peaks was virtually independent of  $c_s$  and  $r_c$ , but was dependent only on the range of the interaction potential. For the solute–solute interaction, we considered the fluctuation in the number of close solute pairs caused by the mutual shift of the crystal inside and outside of the cylindrical glide plane. The fluctuation was a kind of random walk process, and was effective for  $c_s$  higher than a few percent.

The models interpreted the results of MS simulation for fluctuating interaction energy in Fe-Cu alloys under systematically varied conditions. The typical energy height of local peaks exceeded a few electron volts in concentrated alloys, even though the energy of individual solute–defect interaction was around 0.1 eV. The distance between local peaks ranged up to 2 nm. The wavelength of the fluctuation attributable to the solute–defect interaction would be the characteristic length of 1D migration in concentrated alloys. The wavelength was thought to be responsible for the short-range 1D migration of interstitial clusters observed in various alloys under electron irradiation.

### Acknowledgements

This work was supported by a Grant-in-Aid for Scientific Research from the Ministry of Education, Science, and Culture of Japan (No. 21560868). A part of the numerical simulation was performed using the Center for Computational Materials Science, Institute for Materials Research, Tohoku University (Proposal No. 12S0408).

### References

- [1] A.I.J. Foreman, W.J. Phythian, and C.A. English, *Philos. Mag. A* **66**, 671-695 (1992).
- [2] A.F. Calder and D.J. Bacon, *J. Nucl. Mater.* **207**, 25-45 (1993).
- [3] W.J. Phythian, R.E. Stoller, A.E.J. Foreman, A.E. Calder, and D.J. Bacon, *J. Nucl. Mater.* **223**, 245-261 (1995).
- [4] B.D. Wirth, G.R. Odette, D. Maroudas, and G.E. Lucas, *J. Nucl. Mater.* **244**, 185-194 (1997).
- [5] N. Soneda and T. Diaz de la Rubia, *Philos. Mag.* **81**, 331-343 (2001).
- [6] Yu.N. Osetskey, D.J. Bacon, A. Serra, B.N. Singh, and S.I. Golubov, *Philos. Mag.* **83**, 61-91 (2003).

- [7] E. Kuramoto, *J. Nucl. Mater.* **276** (2000) 143-153.
- [8] M. Kiritani, *J. Nucl. Mater.* **251**, 237-251 (1997).
- [9] T. Hayashi, K. Fukumoto, and H. Matsui, *J. Nucl. Mater.* **307-311**, 993-997 (2002).
- [10] K. Arakawa, M. Hatanaka, H. Mori, and K. Ono, *J. Nucl. Mater.* **329-333**, 1194-1198 (2004).
- [11] Y. Satoh, H. Matsui, and T. Hamaoka, *Phys. Rev. B* **77**, 094135 (2008).
- [12] Y. Satoh and H. Matsui, *Philos. Mag.* **89**, 1489-1504 (2009).
- [13] T. Hamaoka, Y. Satoh, and H. Matsui, *J. Nucl. Mater.* **399**, 26-31 (2010).
- [14] Y. Satoh, H. Abe, and S.W. Kim, *Philos. Mag.* **92**, 1129-1148 (2012).
- [15] T. Hamaoka, Y. Satoh, and H. Matsui, *J. Nucl. Mater.* in press.
- [16] D.A. Terentyev, L. Malerba, and M. Hou, *Phys. Rev. B* **75**, 104108 (2007).
- [17] M. Pelfort, Yu.N. Osetsky, and A. Serra, *Philos. Mag. Lett.* **81**, 803-811 (2001).
- [18] S.L. Dudarev, M.R. Gilbert, K. Arakawa, H. Mori, Z. Yao, M.L. Jenkins, and P.M. Derlet, *Phys. Rev. B* **81**, 224107 (2010).
- [19] K. Arakawa, K. Ono, M. Isshiki, K. Mimura, M. Uchikoshi, and H. Mori, *Science* **318**, 956-959 (2007).
- [20] D. Terentyev, N. Anento, A. Serra, V. Jansson, H. Khater, and G. Bonny, *J. Nucl. Mater.* **408**, 272-284 (2011).
- [21] D.A. Terentyev, T.P.C. Klaver, P. Olsson, M.-C. Marinica, F. Williams, C. Domain, and L. Malerba, *Phys. Rev. Lett.* **100**, 145503 (2008).
- [22] S.L. Dudarev, P.M. Derlet, and C.H. Woo, *Nucl. Inst. Meth. Phys. Res. B* **256**, 253-259 (2007).
- [23] G.A. Cottrell, S.L. Dudarev, and R.A. Forrest, *J. Nucl. Mater.* **325**, 195-201 (2004).
- [24] G.J. Ackland, D.J. Bacon, and A.F. Calder, T. Harry, *Philos. Mag.* **75**, 713-732 (1997).
- [25] J. Marian, B.D. Wirth, A. Caro, B. Sadigh, G.R. Odette, J.M. Perlado, and T. Diaz de la Rubia, *Phys. Rev. B* **65**, 144102 (2002).
- [26] A.C. Arokiam, A.V. Barashev, D.J. Bacon, and Y.N. Osetsky, *Philos. Mag.* **87**, 925-943 (2007).
- [27] J. Bastecka and F. Kroupa, *Czech. J. Phys. B* **14**, 443-453 (1964).
- [28] T.S. Hudson, S.L. Dudarev, and A.P. Sutton, *Proc.R. Soc. Lond. A* **460**, 2457-2475 (2004).
- [29] T.A. Khraishi, H.M. Zbib, T. Diaz de la Rubia, and M. Victoria, *Philos. Mag. Lett.*

**81**, 583-593 (2001).

[30] S.L. Dudarev, *Philos. Mag.* **83**, 3577-3597 (2003).

[31] D. Nguyen-Manh, A.P.Horsfield, and S.L. Dudarev, *Phys. Rev. B* **73**, 020101 (2006).

[32] P. Olsson, T.P.C. Klaver, and C. Domain, *Phys. Rev. B* **81**, 054102 (2010).

[33] K. Sato, T. Yoshiie, and Q. Xu, *J. Nucl. Mater.* **367-370**, 382-385 (2007).

[34] D. Terentyev, P. Olsson, L. Malerba, and A.V. Barashev, *J. Nucl. Mater.* **362**, 167-173 (2007).

[35] M. Zaiser, *Philos. Mag.* **81**, 2869-2883 (2002).

[36] D. Terentyev, L. Malerba, and A.V. Barashev, *Philos. Mag. Lett.* **85**, 587-594 (2005).

## Appendix A

This section presents derivation of the power spectrum of the number of solute atoms  $n_j$  in the central core of a cluster. Parseval's theorem shows that the Fourier transform preserves the energy of the original quantity. For real-valued function  $n_j$ ,

$$\frac{1}{L} \sum_{j=0}^{L-1} n_j^2 = \sum_{k=0}^{L-1} |N_k|^2. \quad (\text{A1})$$

The left term of Eq. (A1) represents  $E[n^2]$ . Consequently, the average and the variance of the function  $n_j$  are related to the Fourier coefficients as

$$E[n] = \frac{1}{L} \sum_{j=0}^{L-1} n_j = N_0, \quad V[n] = E[n^2] - E[n]^2 = \sum_{k=1}^{L-1} |N_k|^2. \quad (\text{A2})$$

The power spectrum  $|N_k|^2$  is uniform except for  $k=0$  because of a random variation in  $n_j$ . Then we obtain Eq. (6).

## Appendix B

This section presents a description of a quantitative analysis of the fluctuation in the total number of close solute pairs as an interstitial cluster glide along the Burgers vector. In the model presented in Sec. 4A, the close atomic sites AB that lie across the glide plane are replaced by AC at the dislocation core, as shown in Figure 11 (a). Let the

number of such replacements around the cluster be  $m$  by every 1D migration for the distance  $b$ . For example,  $m$  for the first, second, and third nearest sites is estimated, respectively, as 102, 102, and 252 around 217i, and 18, 18, and 42 for 7i.

We assume a random distribution of solute atoms at concentration  $c_s$ . The probability of finding  $x$  solute atoms on  $m$  sites A is given by the binomial probability distribution  $P_b(x, m, c_s) = \binom{m}{x} c_s^x (1 - c_s)^{m-x}$ . Similarly, the probability of finding  $y (\leq x)$  solute pairs on  $m$  sites AB is given as  $\sum_{x=0}^m P_b(x, m, c_s) P_b(y, x, c_s)$  or  $P_b(y, m, c_s^2)$ . A glide of the cluster for the distance  $b$  induces  $m$  replacements from AB to AC, and the number of close solute pairs will increase, decrease, or stay unchanged depending on the solute distribution on sites A, B, and C. The probability of changing  $\Delta$  solute pairs is expressed as

$$P(\pm\Delta) = \sum_{x=0}^m P_b(x, m, c_s) \sum_{y=0}^m P_b(y, x, c_s) P_b(y + \Delta, x, c_s). \quad (\text{B1})$$

The typical probability distributions are shown in Figure 11(b). The probability takes the maximum at  $\Delta = 0$ , and is symmetrical at  $\Delta = 0$ . Probability  $P(\Delta)$  can be approximated by a normal distribution shown by thin lines for large clusters (with large  $m$ ) at high  $c_s$ .

In successive glide motions of a cluster in random alloys, changes  $\Delta$  in individual steps will be mutually independent. Therefore, the fluctuation in the number of close solute pairs is a kind of random-walk processes. In the well-known ‘simple random walk’, a particle moves +1 or -1 with equal probability at each step. The normal distribution in  $\Delta$  suggests that the present fluctuation can be described better as Brownian motion than as the simple random walk.

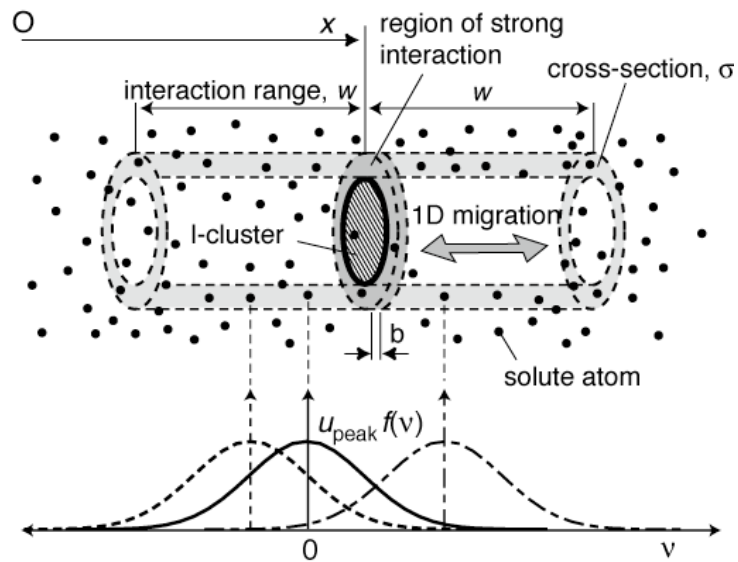


Figure 1. Schematic illustration of the present model describing the total interaction energy between an interstitial cluster and solute atoms in random binary alloys.

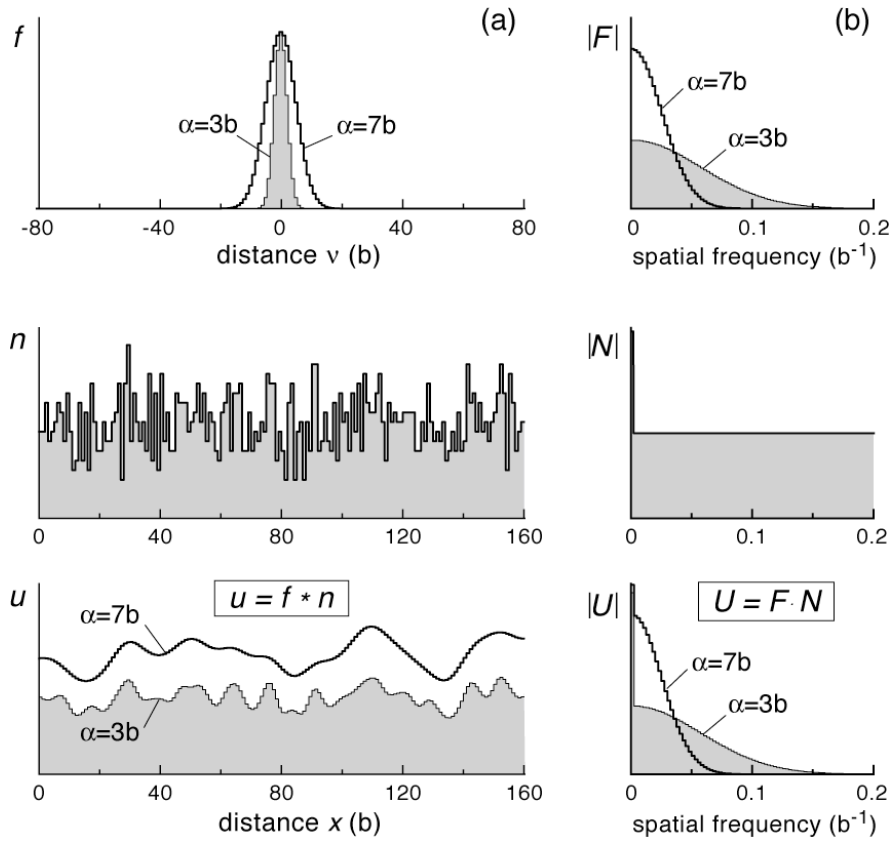


Figure 2. Typical profiles of the interaction potential  $f_j$ , the number of solute atoms  $n_j$  in the region of strong interaction, and total interaction energy  $u_j$ , in (a) the spatial domain and (b) the frequency domain (Fourier spectra). Symbol \* denotes the convolution operation. Parameter  $\alpha$  denotes the interaction range of  $3b$  or  $7b$ .



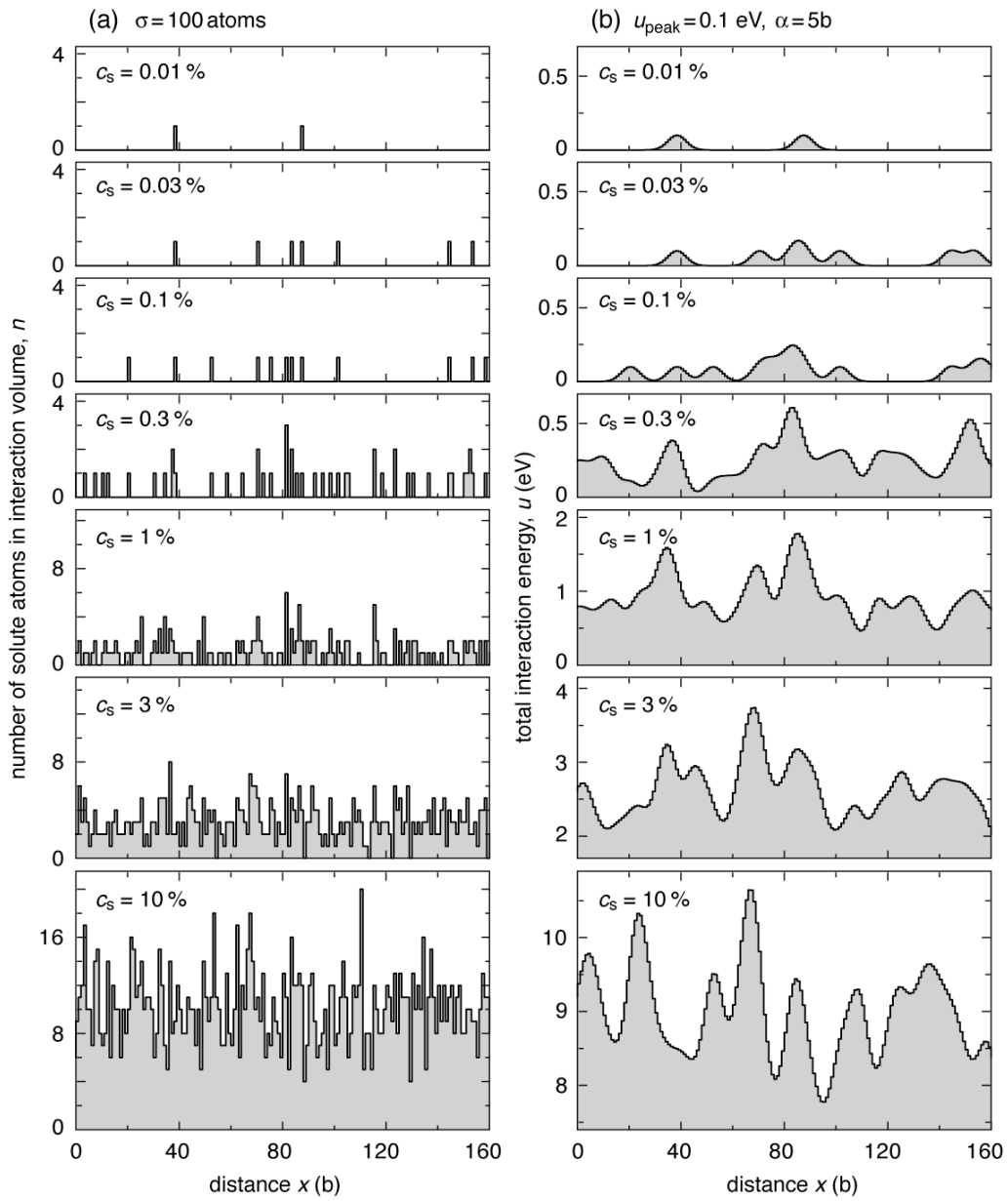


Figure 3. Typical variation of (a) the number of solute atoms  $n_j$  in the region of strong interaction, and (b) the corresponding total interaction energy  $u_j$  with the solute concentration  $c_s$ .  $\sigma = 100$  atoms,  $u_{\text{peak}} = +0.1$  eV, and  $\alpha = 5b$ .

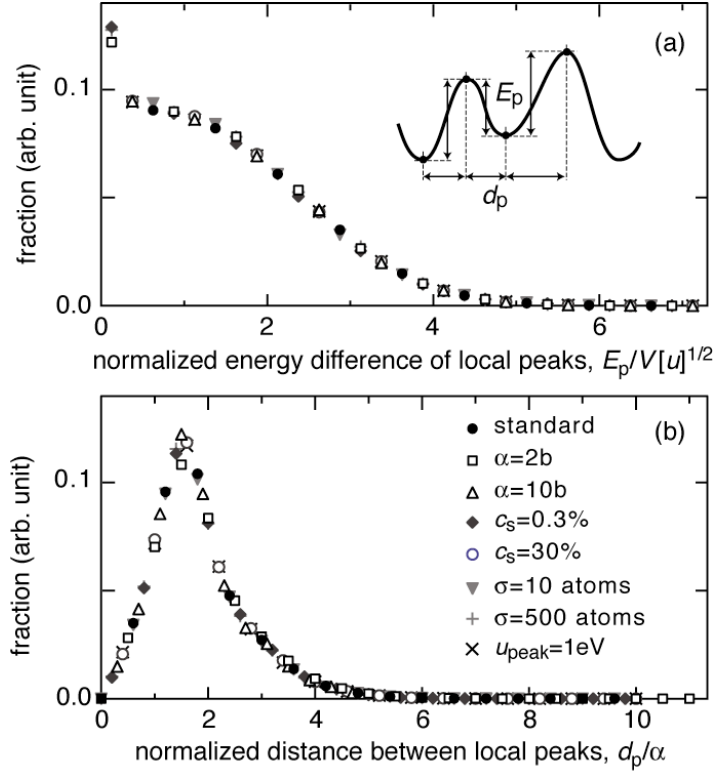


Figure 4. Normalized distributions of (a) the energy difference  $E_p$  and (b) the distance  $d_p$  of the neighboring local peaks in the total interaction energy  $u_j$ . The standard condition was  $\alpha=5b$ ,  $c_s=3\%$ ,  $\sigma=100$  atoms, and  $u_{\text{peak}}=+0.1$  eV. Only the indicated parameter was changed for the other conditions.

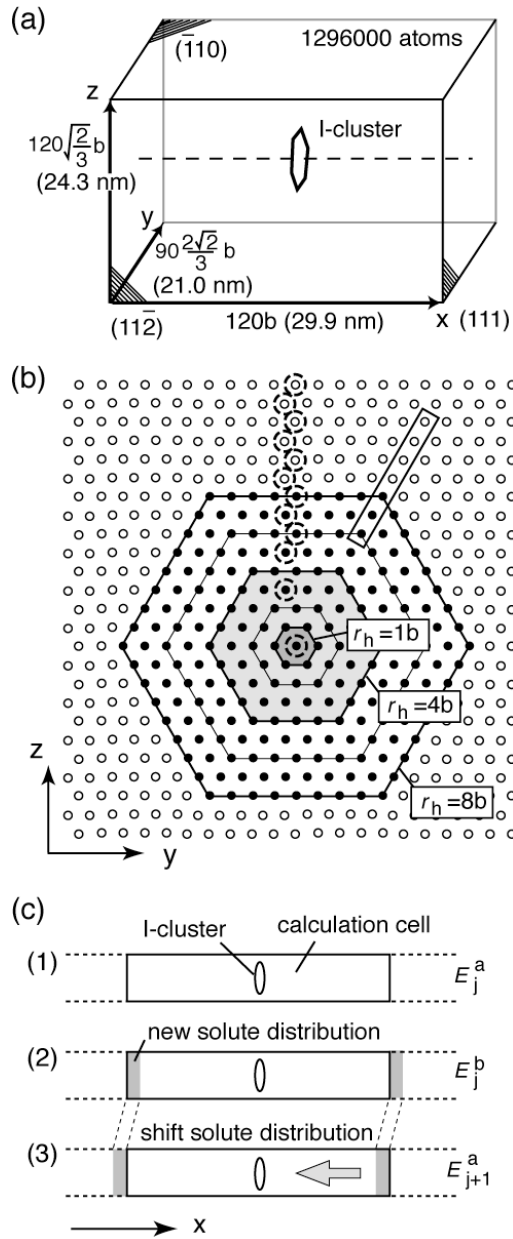


Figure 5. (a) Geometry of the calculation cell used in the atomistic simulations based on the MS method. (b) Configuration of the interstitial cluster observed along the  $x$  direction. Full and open circles respectively correspond to atomic rows with and without the extra plane of 217i. Shaded hexagons show 61i and 71i. (c) Method of calculation of the total interaction energy between an interstitial cluster and solute atoms.

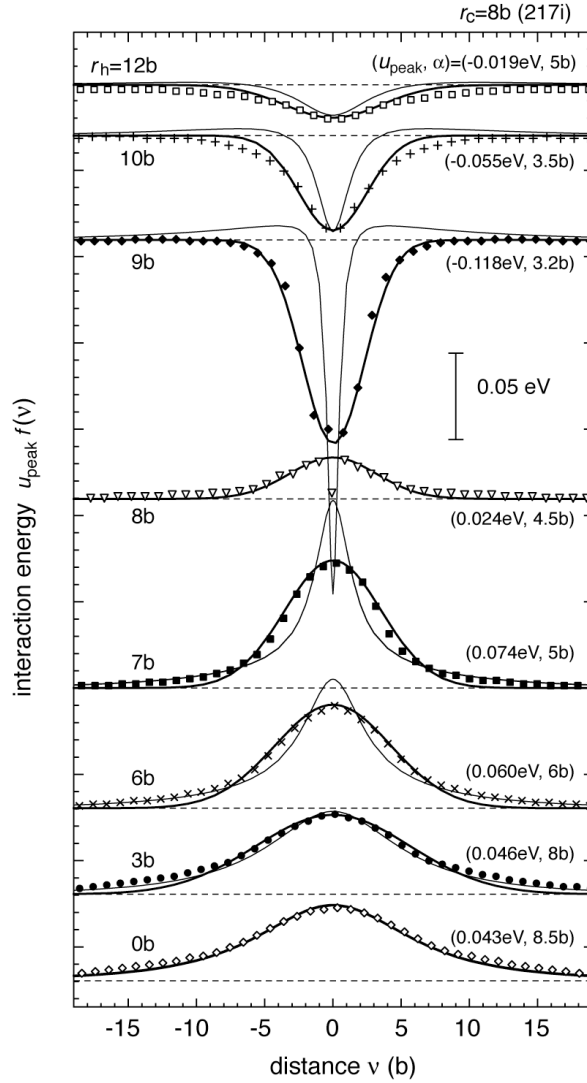


Figure 6. (a) Interaction energy between an interstitial cluster (217i) and a solute copper atom in atomic rows from  $r_h = 0b$  to  $r_h = 12b$  as a function of mutual distance  $v$  in the  $x$  direction (see Figure 1(a)). Symbols show the results of MS calculation. Bold lines are the Gaussian function  $u_{\text{peak}} \exp(-v^2/\alpha^2)$  fitted to the MS results. Interaction energy below the broken lines represents attractive interaction. The solute atom was placed on the atomic rows shown by broken circles in Figure 5(b). Thin lines show the interaction energy between a circular loop and an inclusion according to the elastic theory:  $R = 8.5b$  and  $\delta V = 1.21 \text{ \AA}^3$  in Eq. (10).

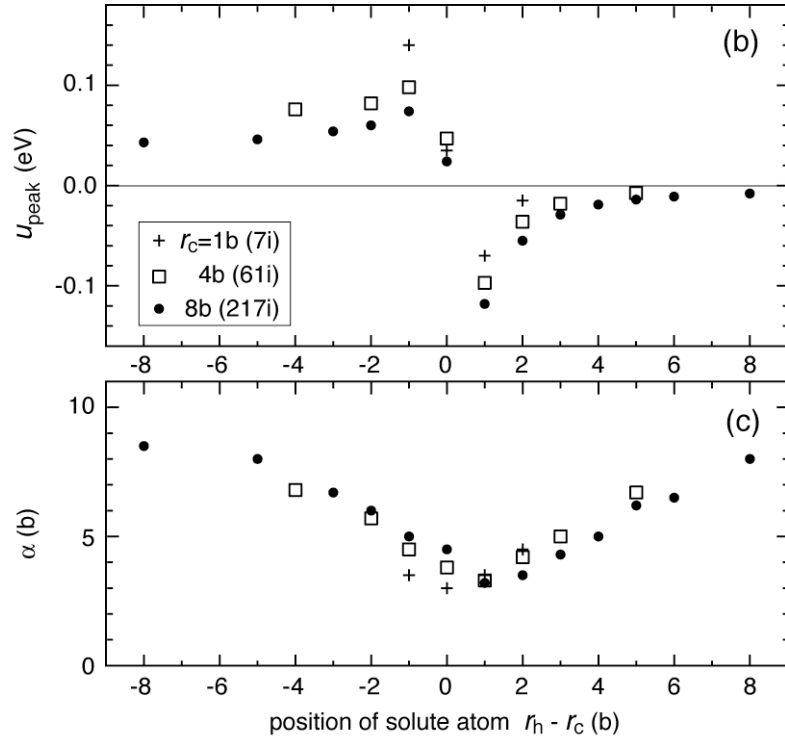


Figure 6. (b) (c) Variation of  $u_{\text{peak}}$  and  $\alpha$  with radii of the interstitial cluster  $r_c$  and of the hexagonal shell  $r_h$  that contains the solute atom.

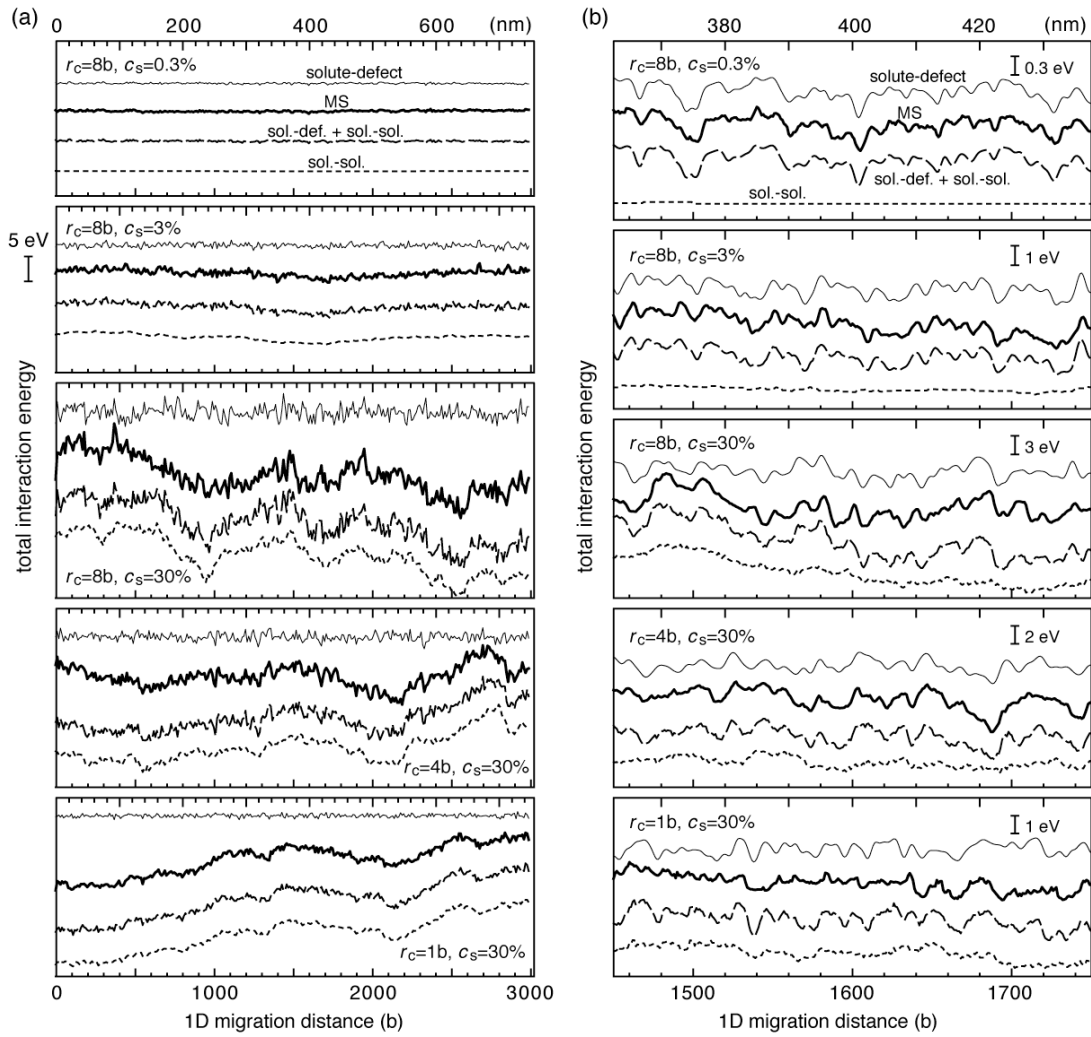


Figure 7. Fluctuation in the total interaction energy between an interstitial cluster and solute atoms in a random alloy as a function of the 1D migration distance of the cluster. Bold lines show results of MS calculations. Thin lines show the superposition of interaction potentials given by Eq. (1’). Dotted lines show contributions of the solute–solute interaction. Results are shown at the common scale in (a), and are magnified for individual conditions in (b).

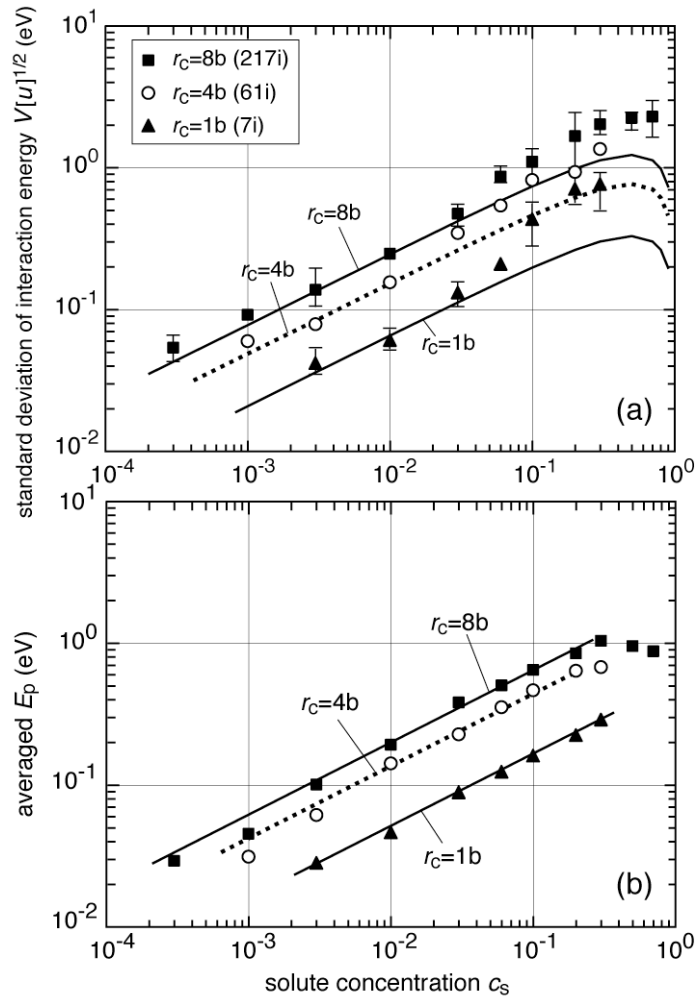


Figure 8. (a) Standard deviation of the total interaction energy as a function of the solute concentration  $c_s$  and the radius  $r_c$  of the interstitial cluster. Symbols and lines respectively show results of MS calculation and superposition of interaction potentials.  $L = 500b$ . (b) Averaged energy difference  $E_p$  of the neighboring peaks in the total interaction energy obtained by MS calculation as a function of  $c_s$  and  $r_c$ . Lines show  $c_s^{1/2}$  relations fitted to the MS results at low  $c_s$ .

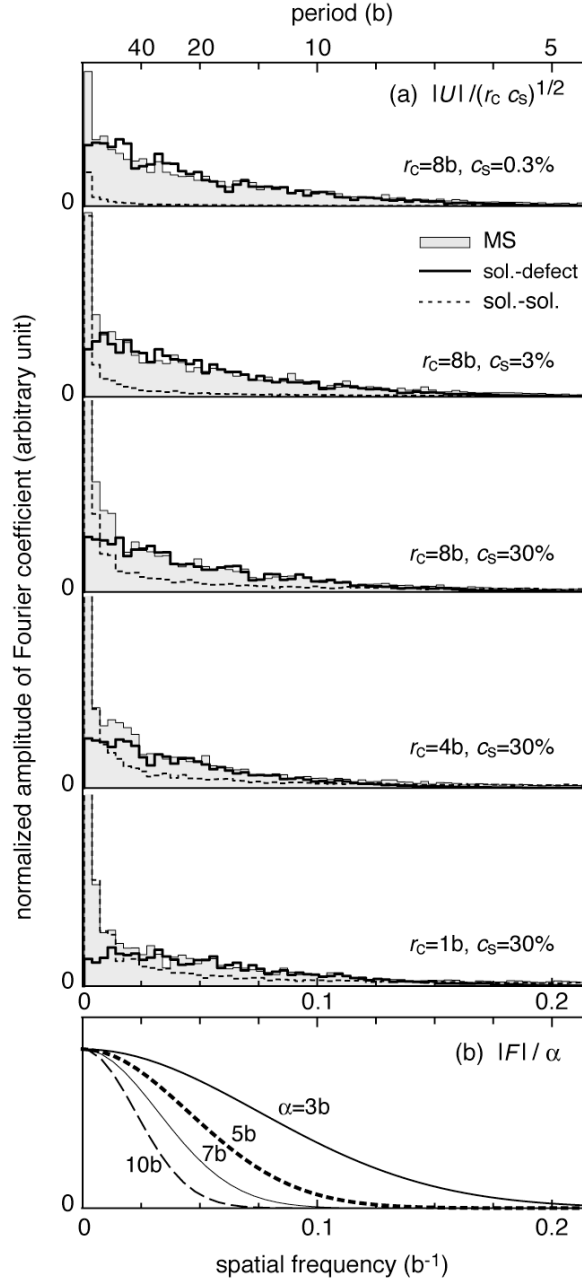


Figure 9. (a) Normalized Fourier spectra of the total interaction energy profiles compared among MS method, superposition of interaction potentials, and solute–solute interaction. The Hamming window function was applied before the Fourier transform to reduce the boundary effect.  $L = 1200b$ . (b) Normalized Fourier spectra of Gaussian functions given by Eq. (5).



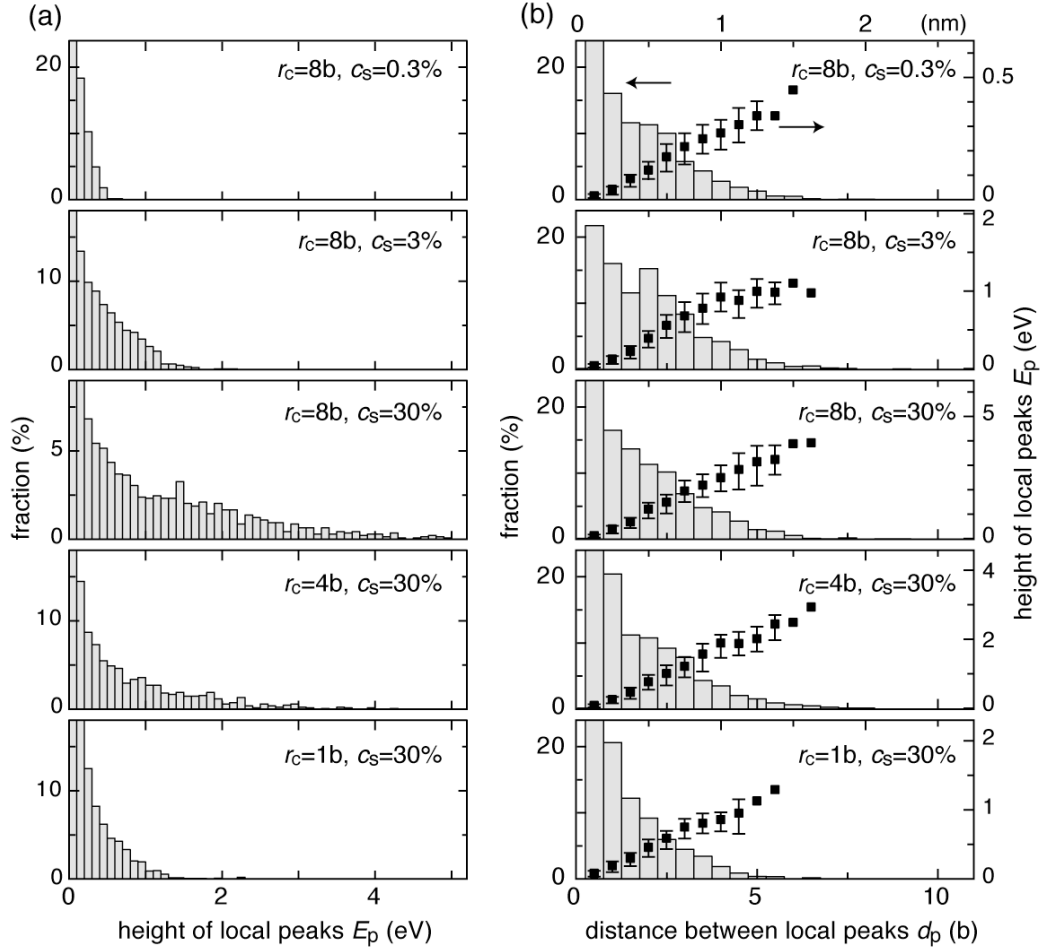


Figure 10. Typical distributions of (a) the energy difference  $E_p$  and (b) the mutual distance  $d_p$  of the neighboring local peaks in the total interaction energy  $u_j$  estimated using MS method. Symbols and error bars in (b) show the average, and the upper and lower quartiles of  $E_p$  for individual bins of the histogram.

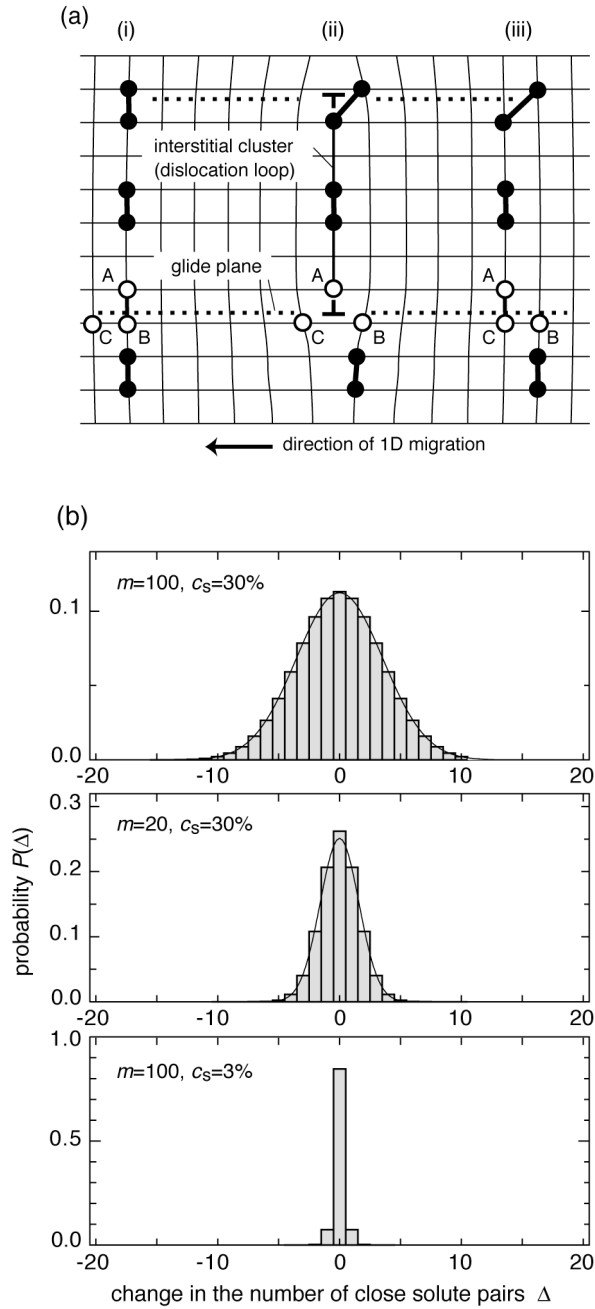


Figure 11. (a) Schematic illustration of the model describing the changes in solute-solute interaction by 1D migration of interstitial clusters in random binary alloys. (b) Typical probability distributions of the change  $\Delta$  in the number of close solute pairs by the 1D migration of interstitial cluster for distance  $b$ . Thin lines show normal distributions fitted to  $P(\Delta)$ .

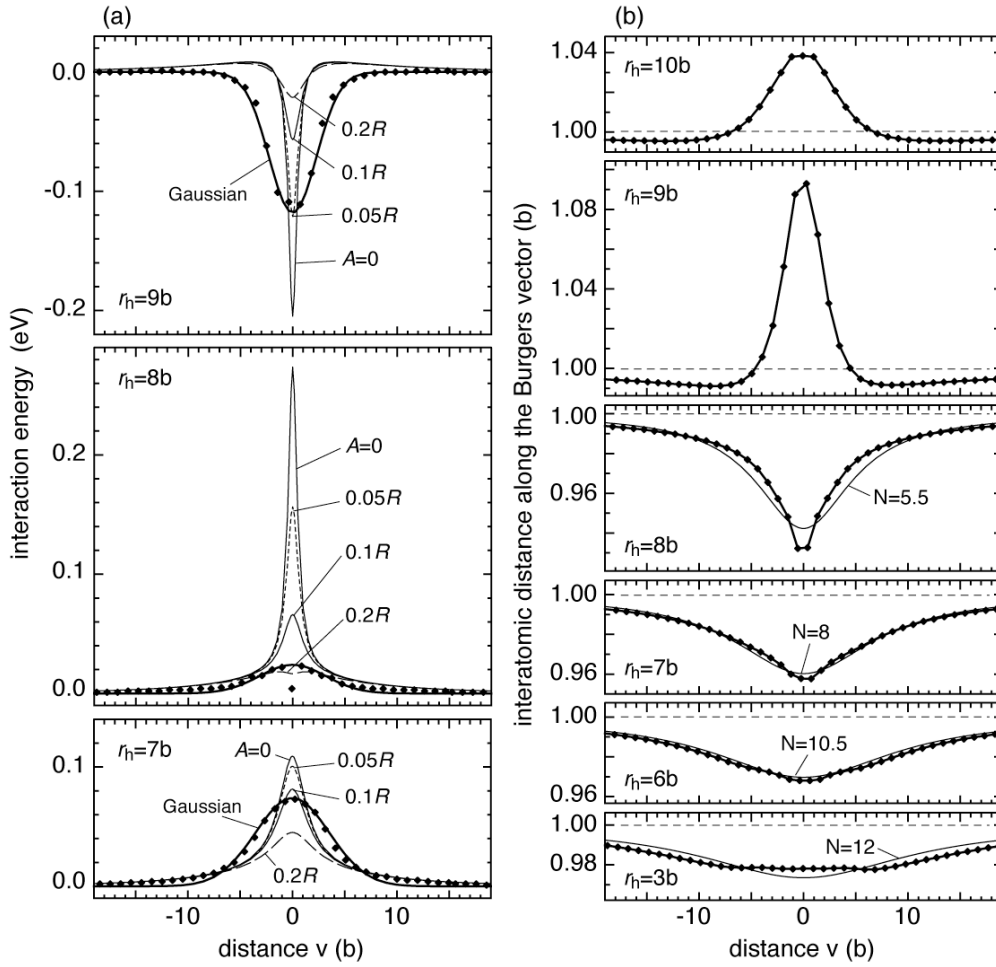


Figure 12. (a) Interaction energy between an interstitial cluster (217i) and a solute copper atom in atomic rows from  $r_h = 7b$  to  $r_h = 9b$  as a function of mutual distance  $v$  in the  $x$  direction. Symbols and bold lines are the MS results and the Gaussian functions, which were already shown in Figure 6(a). Thin lines show the interaction

energy according to the elastic theory [28,29]:  $R = 8.5b$  and  $\delta V = 1.21 \text{ \AA}^3$ . (b)

Interatomic distance along the Burgers vector. Symbols and thick lines are the results of MS calculation for the atomic rows identical to those in Figure 6(a). Thin lines show analytical solutions of the multistring Frenkel-Kontorova model [30]; the parameter  $N$  representing the effective width of a crowdion was fitted to the MS results.